

# Spin-flavor entanglement in $\Lambda_b \rightarrow \Lambda D$ and weak phase extraction

Yong Du,<sup>1,2,\*</sup> Chao-Qiang Geng,<sup>3,†</sup> Xiao-Gang He,<sup>4,5,‡</sup>  
Chia-Wei Liu,<sup>3,§</sup> Sheng-Lin Liu,<sup>3,6,7,¶</sup> and Xin-Yi Liu<sup>3,6,7,\*\*</sup>

<sup>1</sup>*Institute of Modern Physics, Chinese Academy of Sciences, Lanzhou 730000, China*

<sup>2</sup>*School of Nuclear Science and Technology, University of Chinese Academy of Sciences, 19A Yuquan Road, Beijing 100049, China*

<sup>3</sup>*School of Fundamental Physics and Mathematical Sciences, Hangzhou Institute for Advanced Study, UCAS, Hangzhou 310024, China*

<sup>4</sup>*State Key Laboratory of Dark Matter Physics, Tsung-Dao Lee Institute and School of Physics and Astronomy, Shanghai Jiao Tong University, Shanghai 201210, China*

<sup>5</sup>*Key Laboratory for Particle Astrophysics and Cosmology (MOE) & Shanghai Key Laboratory for Particle Physics and Cosmology, Tsung-Dao Lee Institute and School of Physics and Astronomy, Shanghai Jiao Tong University, Shanghai 201210, China*

<sup>6</sup>*Institute of Theoretical Physics, UCAS, Beijing 100190, China*

<sup>7</sup>*University of Chinese Academy of Sciences, Beijing 100190, China*

(Dated: May 12, 2026)

We identify a new spin-flavor entanglement structure in  $\Lambda_b \rightarrow \Lambda D$  decays, formed by the correlation between the  $\Lambda$  spin and the  $D$  flavor states ( $D = D^0, \bar{D}^0, D_1, D_2$ ). The entanglement information is encoded in the decay rates and Lee–Yang parameters of the four neutral- $D$  modes. We then show that the same spin-flavor structure provides a new method to determine the weak phase  $\gamma$ , a key angle of the Cabibbo–Kobayashi–Maskawa unitarity triangle. We find that the experimental uncertainty scales as  $\sigma_\gamma \propto 1/\mathcal{C}$ , where  $\mathcal{C}$  is the Wootters concurrence, thereby quantitatively relating the precision of the weak-phase extraction to the amount of spin-flavor entanglement.

## I. INTRODUCTION

Entanglement provides a useful organizing principle for collider observables, from  $t\bar{t}$  quantum tomography and entanglement at the LHC [1–5] to fermion-pair production at lepton colliders [6–8]. Related spin-correlation systems include  $\Lambda\bar{\Lambda}$  production at BESIII [9–11] and recent baryon-pair entanglement, decay-distillation, and confinement studies [12–17], as well as neutral- $B$  entanglement in  $\Upsilon(4S)$  decays [18]. In this work, we identify a different form of entanglement, the spin-flavor entanglement, in  $\Lambda_b \rightarrow \Lambda D$ , where  $D = D^0, \bar{D}^0, D_1, D_2$ . The neutral- $D$  flavor and the  $\Lambda$  spin form a two-state spin-flavor system whose density matrix can be probed through the decay rates and Lee–Yang parameters [19].

The weak phase  $\gamma$  is the Cabibbo–Kobayashi–Maskawa (CKM) angle [20, 21], defined as the argument of the CKM matrix element  $V_{ij}$  ratio:

$$\gamma \equiv \arg \left[ -\frac{V_{ud}V_{ub}^*}{V_{cd}V_{cb}^*} \right], \quad (1)$$

which appears in the charged-current flavor structure of the Standard Model. Since  $\gamma$  can be determined from

tree-level amplitudes, its theoretical uncertainty is extremely small compared with current and planned experimental precision [22, 23], as demonstrated by the methods employed in  $B \rightarrow D\pi$  and  $B \rightarrow DK$  decays [24–30]. The same interference mechanism is present in  $\Lambda_b \rightarrow \Lambda D$ : the  $V_{ub}V_{cs}^*$  contribution is embedded in  $\Lambda_b \rightarrow \Lambda D^0$ , while the  $V_{cb}V_{us}^*$  contribution is embedded in  $\Lambda_b \rightarrow \Lambda \bar{D}^0$ . Thus, the two flavor-tagged modes carry different CKM phases and interfere when the neutral  $D$  is reconstructed in the CP eigenstates  $|D_1\rangle = (|D^0\rangle + |\bar{D}^0\rangle)/\sqrt{2}$  and  $|D_2\rangle = (|D^0\rangle - |\bar{D}^0\rangle)/\sqrt{2}$ . The weak-phase information is encoded in the entanglement between the  $\Lambda$  spin and the neutral- $D$  flavor. We study this entanglement, depicted in Figure 1, and its role in weak-phase extraction.

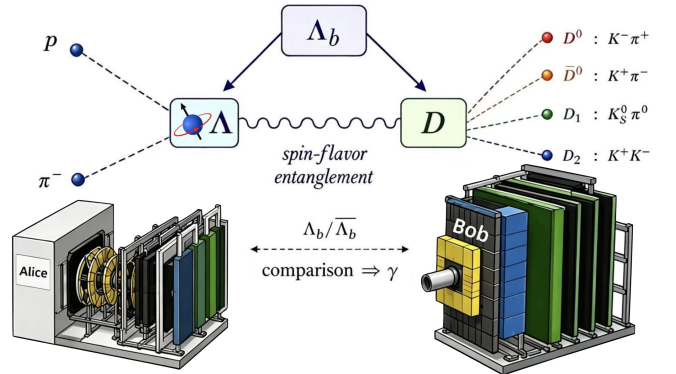


Figure 1: Schematic plot for spin-flavor entanglement in  $\Lambda_b \rightarrow \Lambda D$ , where Alice measures the spin and Bob the flavor.

\* yongdu5@impcas.ac.cn

† cqgeng@ucas.ac.cn

‡ hexg@sjtu.edu.cn

§ chiaweiliu@ucas.ac.cn

¶ liushenglin22@mails.ucas.ac.cn

\*\* liuxinyi24@mails.ucas.ac.cn

## II. SPIN-FLAVOR DENSITY MATRIX AND WEAK-PHASE SENSITIVITY

At the quark level,  $\Lambda_b \rightarrow \Lambda D$  receives two tree-level charged-current contributions. The effective Hamiltonian is written as [31, 32]

$$\mathcal{H}_{\text{eff}} = \frac{G_F}{\sqrt{2}} V_{cb} V_{us}^* \left[ \left( C_1 Q_1^{(c)} + C_2 Q_2^{(c)} \right) + \left| \frac{V_{ub} V_{cs}^*}{V_{cb} V_{us}^*} \right| e^{-i\gamma} \left( C_1 Q_1^{(u)} + C_2 Q_2^{(u)} \right) \right] + \text{h.c.} \quad (2)$$

Here  $G_F$  is the Fermi constant,  $C_i$  are Wilson coefficients, and  $Q_i^{(c)}$  and  $Q_i^{(u)}$  denote the four-quark operators for the  $b \rightarrow \bar{c} \bar{u} s$  and  $b \rightarrow \bar{u} \bar{c} s$  transitions, respectively. Since the initial baryon  $\Lambda_b$  has spin 1/2, the corresponding hadronic matrix elements are most conveniently described in the  $J = 1/2$  partial-wave basis with fixed  $J_z$ ; the  $\Lambda$  and  $J = 1/2$  labels are suppressed below. Details of the quark-operator definitions, the eigenstate normalization  $\mathcal{N}$ , and the relation to the usual Dirac spinor expansion are given in Appendix A. The effective Hamiltonian in Eq. (2) induces the spin-flavor state

$$|\psi, J_z\rangle = \frac{1}{\mathcal{N}} \left[ e^{-i\gamma} |\bar{D}^0\rangle \otimes \chi_{\bar{D}} + |D^0\rangle \otimes \chi_D \right], \quad (3)$$

where

$$\chi_{\bar{D}} = \begin{pmatrix} S_{\bar{D}^0} + P_{\bar{D}^0} \\ S_{\bar{D}^0} - P_{\bar{D}^0} \end{pmatrix}, \quad \chi_D = \begin{pmatrix} S_{D^0} + P_{D^0} \\ S_{D^0} - P_{D^0} \end{pmatrix}, \quad (4)$$

and we use  $S_D$  and  $P_D$  to denote the  $S$ - and  $P$ -wave amplitudes for  $\Lambda_b \rightarrow \Lambda D$ , respectively. The two-component spinors  $\chi_{\bar{D}}$  and  $\chi_D$  are written in the  $\Lambda$ -helicity angular-momentum basis, with  $|J_z, \lambda = +\frac{1}{2}; \Lambda D\rangle = (1, 0)^T$  and  $|J_z, \lambda = -\frac{1}{2}; \Lambda D\rangle = (0, 1)^T$ .

Noting that  $|\psi, J_z\rangle$  lives in the tensor product of the neutral- $D$  flavor and  $\Lambda$  spin spaces, we define the Lee-Yang operators

$$\begin{aligned} \hat{\alpha} &= 2\hat{k} \cdot \vec{s}, & \hat{\beta} &= 2(\vec{J} \times \hat{k}) \cdot \vec{s}, \\ \hat{\gamma} &= 2(\vec{J} - \hat{k} \hat{k} \cdot \vec{J}) \cdot \vec{s}, \end{aligned} \quad (5)$$

where  $\hat{k}$  is the unit vector along the  $\Lambda$  momentum in the  $\Lambda_b$  rest frame, and  $\vec{s}$  is the spin operator of the final-state  $\Lambda$  [33]. These Lee-Yang operators act only on the helicity spinors  $\chi_D$  and  $\chi_{\bar{D}}$ . In the  $\Lambda$ -helicity basis, their action is equivalent to  $\hat{\alpha} \rightarrow \sigma_z$ ,  $\hat{\gamma} \rightarrow \sigma_x$ , and  $\hat{\beta} \rightarrow -\sigma_y$  as demonstrated in Appendix B.

Furthermore, we identify  $\bar{D}^0$  and  $D^0$  as  $(1, 0)^T$  and  $(0, 1)^T$  in flavor space, such that  $\hat{O}_F$  and  $\hat{O}_{12}$  play the roles of  $\sigma_z$  and  $\sigma_x$  in flavor space:

$$\begin{aligned} \hat{O}_F &= |\bar{D}^0\rangle\langle\bar{D}^0| - |D^0\rangle\langle D^0|, \\ \hat{O}_{12} &= |D_1\rangle\langle D_1| - |D_2\rangle\langle D_2|. \end{aligned} \quad (6)$$

The flavor direction  $\sigma_y$  is not directly observable experimentally, since the states  $D^0 \pm i\bar{D}^0$  cannot be tagged. In theory, it can nevertheless be obtained from  $\sigma_y = i\sigma_x \sigma_z$ .

The full spin-flavor density matrix is  $\rho_{J_z} = |\psi, J_z\rangle\langle\psi, J_z|$ . The helicity density matrix for a given neutral- $D$  component is obtained by projecting onto that flavor state:

$$\rho_{J_z, D} = \text{Tr}_D \left( \rho_{J_z} \hat{O}_D \right), \quad (7)$$

and  $\text{Tr}_D$  denotes the partial trace over the two-dimensional neutral- $D$  flavor space. The relevant projectors are  $\hat{O}_{\bar{D}^0, D^0} = (1 \pm \hat{O}_F)/2$  and  $\hat{O}_{D_1, D_2} = (1 \pm \hat{O}_{12})/2$ , where the upper and lower signs refer to the first and second labels, respectively.

A further trace over the helicity space gives the Lee-Yang parameters

$$\xi_D = \frac{\text{Tr}_\lambda(\rho_{J_z, D} \hat{\xi})}{\text{Tr}_\lambda(\rho_{J_z, D})}, \quad \xi \in \{\alpha, \beta, \gamma\}. \quad (8)$$

Thus the hatted quantities  $\hat{\xi}$ , or equivalently the channel-projected operators  $\hat{\xi}_D = \hat{O}_D \hat{\xi}$ , are Lee-Yang operators, while their unhatted expectation values  $\langle \hat{\xi}_D \rangle \in \{\alpha_D, \beta_D, \gamma_D\}$  are Lee-Yang parameters:

$$\begin{aligned} \alpha_D &= \frac{2 \text{Re}(S_D^* P_D)}{|S_D|^2 + |P_D|^2}, & \beta_D &= \frac{2 \text{Im}(S_D^* P_D)}{|S_D|^2 + |P_D|^2}, \\ \gamma_D &= \frac{|S_D|^2 - |P_D|^2}{|S_D|^2 + |P_D|^2}. \end{aligned} \quad (9)$$

Note that  $\gamma_D$  here is a Lee-Yang parameter and should not be confused with the weak phase.

The degree of spin-flavor entanglement is measured by the Wootters concurrence [34]. For the pure state in Eq. (3), it is given by  $\mathcal{C} = 2|\chi_D^T i\sigma_y \chi_{\bar{D}}|/\mathcal{N}^2$ , or equivalently

$$\mathcal{C} = \sqrt{\frac{1 - R_F^2}{2} \left( 1 - \sum_{\xi=\alpha, \beta, \gamma} \xi_{\bar{D}^0} \xi_{D^0} \right)}. \quad (10)$$

Here  $R_F = \langle \hat{O}_F \rangle$  and  $R_{12} = \langle \hat{O}_{12} \rangle$  denote the asymmetries in the flavor and CP-eigenstate bases, respectively,

$$R_F = \frac{\Gamma_{\bar{D}^0} - \Gamma_{D^0}}{\Gamma_{\bar{D}^0} + \Gamma_{D^0}}, \quad R_{12} = \frac{\Gamma_{D_1} - \Gamma_{D_2}}{\Gamma_{D_1} + \Gamma_{D_2}}, \quad (11)$$

where  $\Gamma_D = \Gamma(\Lambda_b \rightarrow \Lambda D)$ . For  $R_{F,12} \neq 1$ , Eq. (10) indicates that the concurrence vanishes only if the two Lee-Yang vectors satisfy  $\xi_{\bar{D}^0} = \xi_{D^0}$ . Because there is only one weak phase in the  $D^0$  and  $\bar{D}^0$  amplitudes, there are no direct CP-odd observables in the flavor-tagged modes  $\Lambda_b \rightarrow \Lambda D^0$  and  $\Lambda_b \rightarrow \Lambda \bar{D}^0$ . Hence  $R_F = \bar{R}_F$ ,  $\xi_{D^0} \xi_{\bar{D}^0} = \bar{\xi}_{\bar{D}^0} \bar{\xi}_{D^0}$ , and from Eq. (10), the CP-conjugate process has the same concurrence.

The observables  $R_{12}$  and  $\bar{R}_{12}$  provide two constraints, but they involve three unknowns:  $|\chi_D^\dagger \chi_D|$ ,  $\arg(\chi_D^\dagger \chi_D)$ , and  $\gamma$ . Hence the weak phase cannot be determined from the rate asymmetries alone. The situation remains the same even if  $\alpha_D$  is determined for all  $D$  modes, although one could still obtain a range for  $\mathcal{C}$  in this case as shown in Eq. (A21). Thus, at least two independent Lee–Yang parameters must be measured in order to overconstrain the system and extract the weak phase.

As a concrete illustration, one may use the projective coordinate of the reconstructed  $\Lambda$ -helicity spinor

$$z_D \equiv \frac{\alpha_D + i\beta_D}{1 + \gamma_D}. \quad (12)$$

The two CP-eigenstate channels then give

$$\gamma = \frac{1}{2} \arg \left[ \frac{(z_{\bar{D}^0} - z_{D_{1,2}})(\bar{z}_{D^0} - \bar{z}_{D_{1,2}})}{(z_{D^0} - z_{D_{1,2}})(\bar{z}_{\bar{D}^0} - \bar{z}_{D_{1,2}})} \right], \quad (13)$$

up to  $\pi$ , with  $\bar{z}_D$  defined from  $\bar{\xi}_D$  in the same way. The quantities inside the argument are cross ratios and are therefore invariant under a common  $SU(2)$  rotation of the helicity basis. The same basis change acts on the Lee–Yang vector through the double-cover map,  $(\gamma_D, -\beta_D, \alpha_D)^T \rightarrow R(\gamma_D, -\beta_D, \alpha_D)^T$ , with  $R \in SO(3)$ . This basis freedom indicates that  $\gamma$  is overconstrained and can thus be extracted without knowing the branching fractions. To use the full information and obtain the strongest constraint, the most direct approach is to determine  $\gamma$  together with the four complex hadronic amplitudes  $S_{\bar{D}^0}$ ,  $P_{\bar{D}^0}$ ,  $S_{D^0}$ , and  $P_{D^0}$  in a simultaneous fit to the measured rates and Lee–Yang parameters.

To estimate the uncertainty in  $\gamma$  extraction, we separate the contributions into off-diagonal and diagonal parts, associated respectively with the  $SU(2)$ -invariant  $\chi_D^T i\sigma_y \chi_D$  and  $\chi_D^\dagger \chi_D$ . The off-diagonal part determines  $\gamma$  with an uncertainty  $\sigma_{\gamma, \text{off}} \simeq \sigma_\xi / \mathcal{C}$ , where  $\sigma_\xi$  is an effective Lee–Yang uncertainty for the rate-weighted transverse coherence. The remaining diagonal information gives only branch-dependent constraints. We summarize its contribution by a dimensionless, non-universal function  $f_{\text{br}}(R_F, \mathcal{C})$ , together with an effective Lee–Yang uncertainty  $\sigma'_\xi$  for the diagonal branch information. These relations are derived in Appendix C. Combining the two contributions through an inverse-variance estimate gives

$$\sigma_\gamma^{\text{full}} \simeq \frac{1}{\mathcal{C}} \left[ \frac{1}{\sigma_\xi^2} + \frac{1}{f_{\text{br}}^2(R_F, \mathcal{C})(\sigma'_\xi)^2} \right]^{-1/2}. \quad (14)$$

The numerical coefficient in the square bracket is analysis dependent and can be modified by rate uncertainties, correlations, and the branch-selection prescription, but the leading behavior  $\sigma_\gamma^{\text{full}} \propto 1/\mathcal{C}$  as  $\mathcal{C} \rightarrow 0$  is unchanged. Note that a similar ill-defined behavior occurs in Eq. (13), since  $z_{D^0} = z_{D_{1,2}}$  and  $\bar{z}_{D^0} = \bar{z}_{D_{1,2}}$  in the limit  $\mathcal{C} = 0$ .

We estimate the statistical resolution of the weak phase with an observable-level Monte Carlo simulation. For

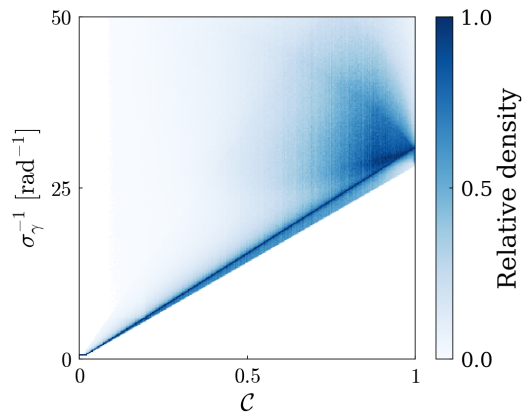


Figure 2: Relative-density distribution of  $(\sigma_\gamma)^{-1}$  versus the spin–flavor concurrence  $\mathcal{C}$ , with  $(\sigma_\gamma)^{-1}$  given in  $\text{rad}^{-1}$ . The lower  $y$  cutoff reflects  $\sigma_\gamma \leq \pi/2$ .

each input concurrence  $\mathcal{C}$ , we generate random  $S$ - and  $P$ -wave amplitudes at fixed  $\mathcal{C}$ , from which the partial widths and Lee–Yang parameters of the four neutral- $D$  modes are obtained. For the full Run-3 data set of LHCb, we take [35–38]

$$N_{\text{tot}} = N_{\Lambda_b} \text{Br}(\Lambda_b^0 \rightarrow \Lambda D) \simeq 3.6 \times 10^7, \quad (15)$$

as the total pre-reconstruction yield. The reconstruction efficiencies vary with the  $D$ -flavor channel and are taken from Ref. [32] and references therein. The channel Lee–Yang operators  $\hat{\xi}_D$  are dichotomic spin observables with outcomes  $\pm 1$ , as shown in Appendix B. Their statistical uncertainties therefore follow from finite samples, as given in Eq. (B8). For illustration, we take  $p_z = 5\%$  as our benchmark. The rate asymmetries  $R_F$  and  $R_{12}$  are obtained from the efficiency-corrected yields, with uncertainties determined by the observed event numbers. We apply the same procedure to the CP-conjugate modes and reconstruct  $\gamma$  in the range  $0 \leq \gamma \leq \pi$ .

Figure 2 shows the relative-density distribution of the scaled inverse resolution  $(\sigma_\gamma)^{-1}$  as a function of  $\mathcal{C}$ . At  $\mathcal{C} = 0$ , the two flavor-tagged helicity spinors become parallel, and the reconstruction of  $\gamma$  becomes ill-conditioned, consistent with the scaling  $\sigma_\gamma \propto 1/\mathcal{C}$  in Eq. (14). The effective lower bound on the resolution is controlled by  $\sigma_\xi/\mathcal{C}$ . When the off-diagonal sensitivity is weaker than the branch-cut uncertainty from the diagonal spinor information, the diagonal contribution becomes ineffective and the full uncertainty follows  $\sigma_\gamma^{\text{full}} \simeq \sigma_\xi/\mathcal{C}$ . Overall, the upward shift of the density band with increasing  $\mathcal{C}$  shows that spin–flavor entanglement is the dominant driver of weak-phase sensitivity.

Using perturbative quantum chromodynamics (pQCD) input [38], we find  $\mathcal{C} = 0.18$ , corresponding to  $\sigma_\gamma \simeq 0.6^\circ$  for  $p_z = 1$  and  $\sigma_\gamma \simeq 11^\circ$  for  $p_z = 5\%$  as inferred from Figure 2 based on our simulation. These values should be compared with the indirect CKM-unity-fit result,  $\gamma = (66.3_{-1.9}^{+0.7})^\circ$ , obtained by CKMfitter [39]. Thus,

the baryonic mode is best regarded as a complementary probe of  $\gamma$ , providing an independent spin-flavor test of the weak phase rather than a direct competitor to existing precision methods.

### III. LOCAL MOMENTUM DENSITY MATRIX AND OBSERVABLE CONCURRENCE

Motivated by the role of concurrence in extracting the weak phase, we investigate the spin-flavor entanglement in  $\Lambda_b \rightarrow \Lambda D$  in this section. While the discussion below focuses on  $\Lambda_b \rightarrow \Lambda D$ , the same setup applies to

its CP counterpart. We start by projecting out the three-momentum eigenstates from the spin-flavor state discussed above, following the standard  $S$ - and  $P$ -wave parametrization of nonleptonic baryon decays [19]:

$$\mathcal{M} = i\bar{u} \left( \mathbf{S} - \frac{\mathbf{P}}{\kappa} \gamma_5 \right) u_b, \quad (16)$$

with  $u_{(b)}$  the Dirac spinors of  $\Lambda_{(b)}$ ,  $\mathbf{S} = (S_{\bar{D}^0}, S_{D^0})^T$ ,  $\mathbf{P} = (P_{\bar{D}^0}, P_{D^0})^T$ , and  $\kappa = \sqrt{(E - m_\Lambda)/(E + m_\Lambda)}$ . Here  $E$  is the energy of  $\Lambda$  in the  $\Lambda_b$  rest frame, and the bold symbols  $\mathcal{M}$ ,  $\mathbf{S}$ , and  $\mathbf{P}$  denote objects in the  $D$ -flavor space. The generalized  $2 \times 2$  differential partial-width matrix  $\mathbf{\Gamma}$  in this  $D$ -flavor space is then written as

$$\frac{\partial \mathbf{\Gamma}}{\partial \cos \theta \partial \phi} = \frac{|\vec{k}|}{64\pi^2 m_{\Lambda_b}^2} \left[ \mathbf{N} (1 + p_z \cos \theta \vec{s} \cdot \hat{r}) + p_z \boldsymbol{\alpha} \cos \theta + \boldsymbol{\alpha} \vec{s} \cdot \hat{r} + p_z \boldsymbol{\beta} \sin \theta \vec{s} \cdot \hat{\phi} - p_z \boldsymbol{\gamma} \sin \theta \vec{s} \cdot \hat{\theta} \right], \quad (17)$$

where  $p_z$ , chosen along the  $\hat{z}$ -axis, is the initial polarization of  $\Lambda_b$ ,  $\hat{r} \equiv \hat{k}$  with  $\hat{k}$  the outgoing direction of  $\Lambda$ , and  $\cos \theta = \hat{z} \cdot \hat{k}$ . The spin of  $\Lambda$  is described by  $\vec{s} = \chi^\dagger \vec{\sigma}_s \chi$ , where  $\vec{\sigma}_s$  are the Pauli matrices in the spin space. The unnormalized flavor-space coupling matrices are directly related to the Lagrangian couplings by  $\mathbf{N} = \mathbf{S}\mathbf{S}^\dagger + \mathbf{P}\mathbf{P}^\dagger$ ,  $\boldsymbol{\alpha} = \mathbf{P}\mathbf{S}^\dagger + \mathbf{S}\mathbf{P}^\dagger$ ,  $\boldsymbol{\beta} = i\mathbf{S}\mathbf{P}^\dagger - i\mathbf{P}\mathbf{S}^\dagger$ , and  $\boldsymbol{\gamma} = \mathbf{S}\mathbf{S}^\dagger - \mathbf{P}\mathbf{P}^\dagger$ . The partial decay width for a specific neutral- $D$  mode is obtained by projecting onto the corresponding flavor state,  $d\Gamma_D = \text{Tr}(d\mathbf{\Gamma} \hat{O}_D)$ , where  $\hat{O}_D$  was defined in Eq. (6).

The normalized density matrix spans  $\mathcal{H}_F \otimes \mathcal{H}_s$ , with  $\mathcal{H}_F$  the flavor and  $\mathcal{H}_s$  the spin Hilbert space, and can be written generally as

$$\rho_{\vec{k}} = \frac{1}{4} \left[ \mathbb{1}_F \otimes \mathbb{1}_s + \mathbb{1}_F \otimes (\vec{B}_s \cdot \vec{\sigma}_s) + (\mathbf{B}_D \cdot \boldsymbol{\sigma}) \otimes \mathbb{1}_s + \sum_{i,j} C_{ij} \sigma_i \otimes \sigma_j^j \right]. \quad (18)$$

Here,  $\vec{B}_s$  and  $\mathbf{B}_D$  are the spin and flavor polarizations, respectively, and  $C_{ij}$  is the spin-flavor correlation matrix.  $i = x, y, z$  labels the flavor direction, and  $j = r, \theta, \phi$  that of the spin. On the one hand,  $\rho_{\vec{k}}$  can be obtained by projecting onto the momentum subspace of  $\rho_{J_z}$  with

$$\rho_{\vec{k}} = \frac{(1+p_z)}{2} \hat{O}_{\vec{k}} \rho_{\frac{1}{2}} \hat{O}_{\vec{k}} + \frac{(1-p_z)}{2} \hat{O}_{\vec{k}} \rho_{-\frac{1}{2}} \hat{O}_{\vec{k}}, \quad (19)$$

using the momentum projector  $\hat{O}_{\vec{k}}$ , for which we refer the reader for more details to Appendix A. On the other hand,  $\rho_{\vec{k}}$  is also directly related to the generalized partial-width matrix  $\mathbf{\Gamma}$ . For instance, the spin polarization  $\vec{B}_s$

of  $\Lambda$  is given by tracing out the flavor subspace:

$$\vec{B}_s = \frac{1}{n} \left[ (\text{Tr}(\boldsymbol{\alpha}) + p_z \text{Tr}(\mathbf{N}) \cos \theta) \hat{r} - p_z \text{Tr}(\boldsymbol{\gamma}) \sin \theta \hat{\theta} + p_z \text{Tr}(\boldsymbol{\beta}) \sin \theta \hat{\phi} \right], \quad (20)$$

where  $n \equiv \text{Tr}(\mathbf{N}) + p_z \text{Tr}(\boldsymbol{\alpha}) \cos \theta$ . For completeness, we also show the results for the flavor polarization  $\mathbf{B}_D$  and the correlation matrix  $C_{ij}$ :

$$\mathbf{B}_D^i = \frac{\text{Tr}[(\mathbf{N} + p_z \cos \theta \boldsymbol{\alpha}) \boldsymbol{\sigma}_i]}{n}, \quad (21)$$

$$C_{ij} = \frac{1}{n} \text{Tr} \left\{ \boldsymbol{\sigma}_i \left[ (\mathbf{N} p_z \cos \theta + \boldsymbol{\alpha}) \delta_j^r + p_z \boldsymbol{\beta} \sin \theta \delta_j^\phi - p_z \boldsymbol{\gamma} \sin \theta \delta_j^\theta \right] \right\}.$$

with  $\delta_j^r$ ,  $\delta_j^\theta$ , and  $\delta_j^\phi$  the Kronecker deltas in the spin-index space. Again, we stress that experimentally the flavor- $y$  component cannot be tagged, and elements of the polarization vectors and the correlation matrix are directly related to the Lee-Yang parameters and the asymmetries through the identities

$$\text{Tr}(\boldsymbol{\sigma}_x \boldsymbol{\xi}) = \Gamma_{D_1} \xi_{D_1} - \Gamma_{D_2} \xi_{D_2}, \quad (22)$$

$$\text{Tr}(\boldsymbol{\sigma}_z \boldsymbol{\xi}) = \Gamma_{\bar{D}^0} \xi_{\bar{D}^0} - \Gamma_{D^0} \xi_{D^0}.$$

These quantities can be determined numerically once the  $S$ - and  $P$ -wave amplitudes are specified.

The size of spin-flavor entanglement in this momentum eigenstate is then quantified by [34]

$$\mathcal{C}_{\vec{k}} = \max(0, 2\lambda_{\max} - \text{Tr} \mathcal{R}), \quad (23)$$

with  $\mathcal{R} = \sqrt{\sqrt{\rho_{\vec{k}}} (\boldsymbol{\sigma}_y \otimes \boldsymbol{\sigma}_s^\theta) \rho_{\vec{k}}^* (\boldsymbol{\sigma}_y \otimes \boldsymbol{\sigma}_s^\theta) \sqrt{\rho_{\vec{k}}}}$  and  $\lambda_{\max}$  the largest eigenvalue of  $\mathcal{R}$ . Here  $\mathcal{C}_{\vec{k}}$  denotes the concurrence of the spin-flavor density matrix in the fixed- $\vec{k}$

momentum-eigenstate subspace. A direct Bell test is forbidden at colliders because the relevant spin and flavor components are not directly measurable [47]. Nevertheless, CHSH parameters can still diagnose entanglement and the collider-accessible construction is given by Eq. (A12) in Appendix A.

We show the theoretical prediction of  $\mathcal{C}_{\bar{k}}$  in Figure 3, using recent theoretical  $S$ - and  $P$ -wave amplitude results from pQCD [38]. The plot shows that  $\mathcal{C}_{\bar{k}}$  is rather sensitive to the initial polarization  $p_z$  of  $\Lambda_b$ : (1) For  $p_z = 0$ , when the decaying  $\Lambda_b$  is unpolarized, it is clear from Eq. (17), or equivalently from Eqs. (18)–(21), that the state becomes separable such that  $\mathcal{C}_{\bar{k}} = 0$ . As a consequence, the extraction of  $\gamma$  becomes inaccessible, which echoes that  $\beta_D$  and  $\gamma_D$  cannot be measured at  $p_z = 0$ . (2) For  $p_z \neq 0$ , non-vanishing spin–flavor entanglement can generically be induced, and maximal  $\mathcal{C}_{\bar{k}}$  of  $\mathcal{O}(0.5)$  can be achieved in a wide range of the decay angle  $\theta$ , except when  $\theta$  is close to 0 or  $\pi$ , i.e., the transverse production plane of  $\Lambda_b$ .

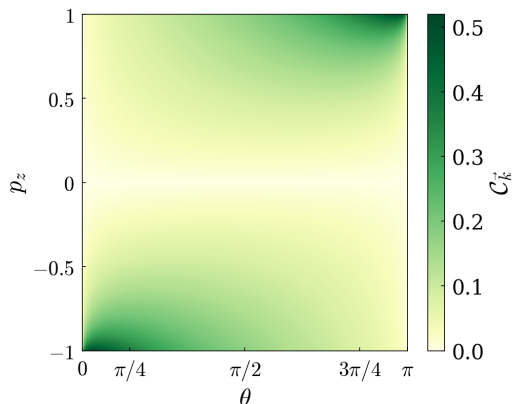


Figure 3: Theoretical prediction of the concurrence  $\mathcal{C}_{\bar{k}}$  from the final-state spin–flavor entanglement in  $\Lambda_b \rightarrow \Lambda D$ .

Historically,  $p_z$  has been measured by various experiments at LEP and, more recently, by the CMS and LHCb collaborations. These results are summarized in Table I, and are all consistent with vanishing  $\Lambda_b$  polarization. The dominant uncertainty in these measurements is statistical, and is expected to be substantially reduced, for example, by the Tera- $Z$  runs of future lepton colliders such as CEPC [45] and FCC-ee [46]. Such an improved measurement of  $p_z$  could in turn increase the accessible value of  $\mathcal{C}_{\bar{k}}$  and thereby improve the precision of the  $\gamma$  determination.

Exp.	$p_z$	Ref.
ALEPH	$-0.23 \pm 0.23$	[40]
OPAL	$-0.56 \pm 0.19$	[41]
DELPHI	$-0.49 \pm 0.35$	[42]
CMS	$0.00 \pm 0.08$	[43]
LHCb	$[-0.06, 0.05]_{\sqrt{s}=7 \text{ TeV}}$	[44]
	$[-0.04, 0.05]_{\sqrt{s}=8 \text{ TeV}}$	[44]
	$[-0.01, 0.07]_{\sqrt{s}=13 \text{ TeV}}$	[44]

Table I: A summary of existing  $p_z$  measurements at the lepton and the hadron colliders. The statistical and systematical uncertainties are summed in quadrature except in the LHCb case, the latter of which stands for the interval at the 68% confidence level.

#### IV. CONCLUSION

We have identified a new spin–flavor entanglement structure in  $\Lambda_b \rightarrow \Lambda D$  that correlates the  $\Lambda$  spin and the neutral- $D$  flavor. The corresponding information is encoded in the decay rates and Lee–Yang parameters of the  $D = D^0, \bar{D}^0, D_1, D_2$  modes. This structure is both a quantum feature of the final state and a probe of weak-phase sensitivity: the weak-phase uncertainty scales as  $\sigma_\gamma \propto 1/\mathcal{C}$ , where  $\mathcal{C}$  is the spin–flavor concurrence. Thus, when the spin and flavor degrees of freedom become separable, the extraction of  $\gamma$  becomes ill-conditioned. In particular,  $\gamma$  cannot be extracted from branching fractions alone.

We also projected the same state onto local momentum wave packets and constructed the corresponding spin–flavor density matrix. This local description shows how the initial polarization and decay angle control the observable concurrence. A realistic experimental implementation should use a global likelihood for the rates, Lee–Yang parameters, efficiencies, and covariances, but the central conclusion is basis independent:  $\gamma$  is best resolved when the final-state spin and flavor degrees of freedom are strongly entangled.

#### ACKNOWLEDGEMENTS

This work is supported in part by the National Natural Science Foundation of China under Grant Nos. 12090064, 12375088, W2441004, 12547104, and 12575096, the Fundamental Research Funds for the Central Universities, and the CAS One Hundred Talent Program.

- [1] Y. Afik and J. R. M. de Nova, *Eur. Phys. J. Plus* **136**, 907 (2021), arXiv:2003.02280.  
 [2] G. Aad *et al.* (ATLAS Collaboration), *Nature* **633**, 542 (2024), arXiv:2311.07288.

- [3] A. Hayrapetyan *et al.* (CMS Collaboration), *Rept. Prog. Phys.* **87**, 117801 (2024), arXiv:2406.03976.  
 [4] J. Gu, S. J. Lin, D. Y. Shao, L. T. Wang, and S. X. Yang, arXiv:2510.13951.

- [5] T. Han, M. Low, N. McGinnis and S. Su, JHEP **05**, 081 (2025) arXiv:2412.21158.
- [6] Y. J. Fang, A. Bhoonah, K. Cheng, T. Han, Y. Liu and H. Zhang, arXiv:2604.11887.
- [7] K. Cheng and B. Yan, Phys. Rev. Lett. **135**, 1 (2025) arXiv:2501.03321.
- [8] Q. H. Cao, G. Li, X. K. Wen and B. Yan, arXiv:2509.18276.
- [9] M. Ablikim *et al.* (BESIII Collaboration), Nature Phys. **15**, 631 (2019), arXiv:1808.08917.
- [10] E. Perotti, G. Fäldt, A. Kupsc, S. Leupold, and J. J. Song, Phys. Rev. D **99**, 056008 (2019), arXiv:1809.04038.
- [11] S. Wu, C. Qian, Q. Wang and X. R. Zhou, Phys. Rev. D **110**, 054012 (2024) arXiv:2406.16298.
- [12] Y. Du, X. G. He, C. W. Liu and J. P. Ma, Eur. Phys. J. C **85**, 1255 (2025), arXiv:2409.15418.
- [13] S. J. Lin, M. J. Liu, D. Y. Shao and S. Y. Wei, JHEP **11**, 082 (2025), arXiv:2507.15387.
- [14] C. Chen and J. J. Xie, arXiv:2603.24011.
- [15] H. L. Feng, H. Tang, W. Z. Guo and Q. Qin, Phys. Rev. D **112**, 036020 (2025), arXiv:2504.15798.
- [16] B. E. Aboona *et al.* (STAR Collaboration), Nature **650**, 65 (2026), arXiv:2506.05499.
- [17] L. Oliva, Q. Wang, and X. N. Wang, arXiv:2603.10427.
- [18] A. Go *et al.* (Belle Collaboration), Phys. Rev. Lett. **99**, 131802 (2007), arXiv:quant-ph/0702267.
- [19] T. D. Lee and C. N. Yang, Phys. Rev. **108**, 1645 (1957).
- [20] N. Cabibbo, Phys. Rev. Lett. **10**, 531 (1963).
- [21] M. Kobayashi and T. Maskawa, Prog. Theor. Phys. **49**, 652 (1973).
- [22] S. Navas *et al.* (Particle Data Group), Phys. Rev. D **110**, 030001 (2024).
- [23] J. Brod and J. Zupan, JHEP **01**, 051 (2014), arXiv:1308.5663.
- [24] M. Gronau and D. Wyler, Phys. Lett. B **265**, 172 (1991).
- [25] M. Gronau and D. London, Phys. Lett. B **253**, 483 (1991).
- [26] D. Atwood, I. Dunietz, and A. Soni, Phys. Rev. Lett. **78**, 3257 (1997), arXiv:hep-ph/9612433.
- [27] D. Atwood, I. Dunietz, and A. Soni, Phys. Rev. D **63**, 036005 (2001), arXiv:hep-ph/0008090.
- [28] A. Giri, Y. Grossman, A. Soffer, and J. Zupan, Phys. Rev. D **68**, 054018 (2003), arXiv:hep-ph/0303187.
- [29] R. Aaij *et al.* (LHCb Collaboration), JHEP **12**, 141 (2021), arXiv:2110.02350.
- [30] I. Adachi *et al.* (Belle and Belle II Collaborations), JHEP **10**, 143 (2024), arXiv:2404.12817.
- [31] G. Buchalla, A. J. Buras and M. E. Lautenbacher, Rev. Mod. Phys. **68**, 1125 (1996), arXiv:hep-ph/9512380.
- [32] C. Q. Geng, X. N. Jin, C. W. Liu, Z. Y. Wei and J. Zhang, Phys. Lett. B **834**, 137429 (2022) arXiv:2206.00348.
- [33] A. McKerrell, *Nuovo Cim* **34**, 1289 (1964).
- [34] W. K. Wootters, Phys. Rev. Lett. **80**, 2245 (1998).
- [35] R. Aaij *et al.* (LHCb Collaboration), Phys. Rev. Lett. **118**, 052002 (2017); Erratum: Phys. Rev. Lett. **119**, 169901 (2017), arXiv:1612.05140.
- [36] S. Vecchi (LHCb Collaboration), EPJ Web Conf. **192**, 00024 (2018).
- [37] R. Aaij *et al.* (LHCb Collaboration), Phys. Rev. D **100**, 031102 (2019), arXiv:1902.06794.
- [38] Z. Rui, Z. T. Zou, Y. Li and Y. Li, arXiv:2604.17877.
- [39] A. Hocker, H. Lacker, S. Laplace and F. Le Diberder, Eur. Phys. J. C **21**, 225-259 (2001) arXiv:hep-ph/0104062; J. Charles *et al.* [CKMfitter Group], Eur. Phys. J. C **41**, 1-131 (2005) arXiv:hep-ph/0406184.
- [40] D. Buskulic *et al.* [ALEPH], Phys. Lett. B **365**, 437-447 (1996).
- [41] G. Abbiendi *et al.* [OPAL], Phys. Lett. B **444**, 539-554 (1998) arXiv:hep-ex/9808006.
- [42] P. Abreu *et al.* [DELPHI], Phys. Lett. B **474**, 205-222 (2000).
- [43] A. M. Sirunyan *et al.* [CMS], Phys. Rev. D **97**, no.7, 072010 (2018) [arXiv:1802.04867 [hep-ex]].
- [44] R. Aaij *et al.* [LHCb], JHEP **06**, 110 (2020) arXiv:2004.10563.
- [45] J. B. Guimarães da Costa *et al.* [CEPC Study Group], arXiv:1811.10545.
- [46] A. Abada *et al.* [FCC], Eur. Phys. J. ST **228**, 261-623 (2019).
- [47] S. A. Abel, M. Dittmar, and H. K. Dreiner, Phys. Lett. B **280**, 304 (1992).
- [48] J. F. Clauser, M. A. Horne, A. Shimony, and R. A. Holt, Phys. Rev. Lett. **23**, 880 (1969).
- [49] R. Horodecki, P. Horodecki, and M. Horodecki, Phys. Lett. A **200**, 340 (1995).

## Appendix A: Eigenstate decomposition

Before turning to the state decomposition, we recall the quark-level Hamiltonian used in the main text:

$$\mathcal{H}_{\text{eff}} = \frac{G_F}{\sqrt{2}} V_{cb} V_{us}^* \left[ C_1 Q_1^{(c)} + C_2 Q_2^{(c)} + \left| \frac{V_{ub} V_{cs}^*}{V_{cb} V_{us}^*} \right| e^{-i\gamma} \left( C_1 Q_1^{(u)} + C_2 Q_2^{(u)} \right) \right] + \text{h.c.} \quad (\text{A1})$$

With color indices  $\alpha, \beta$ , the four-quark operators are

$$\begin{aligned} Q_1^{(c)} &= (\bar{c}_\alpha b_\beta)_{V-A} (\bar{s}_\beta u_\alpha)_{V-A}, & Q_2^{(c)} &= (\bar{c}_\alpha b_\alpha)_{V-A} (\bar{s}_\beta u_\beta)_{V-A}, \\ Q_1^{(u)} &= (\bar{u}_\alpha b_\beta)_{V-A} (\bar{s}_\beta c_\alpha)_{V-A}, & Q_2^{(u)} &= (\bar{u}_\alpha b_\alpha)_{V-A} (\bar{s}_\beta c_\beta)_{V-A}. \end{aligned} \quad (\text{A2})$$

Here  $(\bar{q}_\alpha q_\beta)_{V-A} \equiv \bar{q}_\alpha \gamma^\mu (1 - \gamma_5) q_\beta$ . The  $S$ - and  $P$ -wave amplitudes are defined through the momentum-space matrix element, with  $\vec{k}$  the outgoing  $\Lambda$  momentum in the  $\Lambda_b$  rest frame and  $\kappa = \sqrt{(E - m_\Lambda)/(E + m_\Lambda)}$ :

$$\mathcal{M}_D(J_z) = \langle \vec{k}, \vec{s}; \Lambda D | \mathcal{H}_{\text{eff}} | \Lambda_b, J_z \rangle = i \bar{u}(\vec{k}, \vec{s}) \left( S_D - \frac{P_D}{\kappa} \gamma_5 \right) u_b(J_z). \quad (\text{A3})$$

We start with the derivation of momentum eigenstates and then proceed to angular-momentum eigenstates.

### 1. Momentum eigenstates

For a  $\Lambda_b$  state with fixed  $J_z$ , the final state is projected onto momentum eigenstates as

$$|\psi_{J_z, \vec{s}, \vec{k}}\rangle = \hat{O}_{\vec{k}, \vec{s}} \mathcal{H}_{\text{eff}} |\Lambda_b, J_z\rangle, \quad (\text{A4})$$

with the projector

$$\hat{O}_{\vec{k}, \vec{s}} = \sum_D |\vec{k}, \vec{s}; \Lambda D\rangle \langle \vec{k}, \vec{s}; \Lambda D|. \quad (\text{A5})$$

Here  $\vec{s}$  denotes the spin of  $\Lambda$ , and the state  $|\psi_{J_z, \vec{s}, \vec{k}}\rangle$  has not been normalized. It should be emphasized that  $|\psi_{J_z, \vec{s}, \vec{k}}\rangle$  is not itself an eigenstate of  $J_z$ . Rather, it is the fixed- $\vec{k}$ , fixed- $\vec{s}$  component projected out from the decay product of a fixed- $J_z$  state. The density matrix for an initially polarized  $\Lambda_b$  is the incoherent mixture

$$\rho(\vec{s}) = \frac{1+p_z}{2} |\psi_{\frac{1}{2}, \vec{s}, \vec{k}}\rangle \langle \psi_{\frac{1}{2}, \vec{s}, \vec{k}}| + \frac{1-p_z}{2} |\psi_{-\frac{1}{2}, \vec{s}, \vec{k}}\rangle \langle \psi_{-\frac{1}{2}, \vec{s}, \vec{k}}|. \quad (\text{A6})$$

The corresponding matrix element is

$$|\psi_{J_z, \vec{s}, \vec{k}}\rangle \langle \psi_{J_z, \vec{s}, \vec{k}}| = \sum_{D, D'} |\vec{k}, \vec{s}; \Lambda D\rangle \langle \vec{k}, \vec{s}; \Lambda D'| \mathcal{M}_D(J_z) \mathcal{M}_{D'}(J_z)^*. \quad (\text{A7})$$

We note that

$$\mathcal{M}_D(J_z) \mathcal{M}_{D'}^*(J_z) = \bar{u}(\vec{s}) \left( S_D - \frac{P_D}{\kappa} \gamma_5 \right) u_b(J_z) \bar{u}_b(J_z) \left( S_{D'}^* + \frac{P_{D'}^*}{\kappa} \gamma_5 \right) u(\vec{s}) \quad (\text{A8})$$

has the same structure as in the usual derivation [19]. For example,

$$\mathcal{M}_D \mathcal{M}_{D'}^* = \frac{1}{4} \text{Tr} \left[ (\not{p}_\Lambda + m_\Lambda) (1 + \gamma_5 \not{s}) \left( S_D - \frac{P_D}{\kappa} \gamma_5 \right) (\not{p}_b + m_{\Lambda_b}) (1 + \gamma_5 \not{s}_b) \left( S_{D'}^* + \frac{P_{D'}^*}{\kappa} \gamma_5 \right) \right], \quad (\text{A9})$$

where  $s_b = (0, 0, 0, J_z)$ . The trace can be evaluated straightforwardly using MATHEMATICA.

To express the result in matrix form, we adopt the basis

$$|\vec{k}, \vec{s}; \Lambda D^0\rangle = (1, 0)^T, \quad |\vec{k}, \vec{s}; \Lambda \bar{D}^0\rangle = (0, 1)^T. \quad (\text{A10})$$

Then the flavor density matrix elements are

$$\rho = \begin{pmatrix} \mathcal{M}_{D^0} \mathcal{M}_{D^0}^* & \mathcal{M}_{D^0} \mathcal{M}_{\bar{D}^0}^* \\ \mathcal{M}_{\bar{D}^0} \mathcal{M}_{D^0}^* & \mathcal{M}_{\bar{D}^0} \mathcal{M}_{\bar{D}^0}^* \end{pmatrix}. \quad (\text{A11})$$

In terms of Eq. (16),  $\rho \propto \mathbf{M} \mathbf{M}^\dagger$  and, since  $d\Gamma \propto \rho$ , Eq. (17) follows immediately.

From the density matrix setup above, the Clauser–Horne–Shimony–Holt (CHSH) parameter  $\mathcal{B}$  [48, 49] can be computed from the Horodecki bound,  $\mathcal{B} \leq 2\sqrt{\mu_1^2 + \mu_2^2}$ , where  $\mu_i^2$  are the eigenvalues of  $\mathbf{C} \mathbf{C}^T$ , ordered as  $\mu_1^2 \geq \mu_2^2 \geq \mu_3^2$ . Since the flavor- $y$  direction is experimentally inaccessible, the physical CHSH parameter is obtained from the  $x$  and  $z$  flavor components:

$$\begin{aligned} \max[\mathcal{B}_{\text{phys}}] &= 2 \sqrt{\sum_{i=x,z} (\hat{\mathbf{C}} \hat{\mathbf{C}}^T)_{ii}} \\ &= \frac{2}{1 + p_z \alpha_{\text{av}} \cos \theta} \sqrt{(p_z \cos \theta R_{12} + \alpha_{12})^2 + (p_z \cos \theta R_F + \alpha_F)^2 + p_z^2 \sin^2 \theta (\beta_{12}^2 + \beta_F^2 + \gamma_{12}^2 + \gamma_F^2)}, \end{aligned} \quad (\text{A12})$$

with  $\alpha_{\text{av}} = \frac{1}{2} [(1 + R_F) \alpha_{\bar{D}^0} + (1 - R_F) \alpha_{D^0}]$ . At  $p_z = 0$ ,  $\mathbf{C} \mathbf{C}^T$  becomes a rank-one matrix, such that  $\mu_2^2 = 0$  and  $\mathcal{B} \leq 2$ . In the same limit, the concurrence also vanishes. The maximal value obtained by varying the Lee–Yang parameters is

$$\max_{\xi} [\mu_1^2 + \mu_2^2] = 1 + \frac{p_z^2 \sin^2 \theta}{1 - p_z^2 \cos^2 \theta}. \quad (\text{A13})$$

A simple example that saturates this bound for  $p_z = 1$  at  $\theta = \pi/2$  is given by  $S_{D^0} = iP_{\bar{D}^0}$  and  $P_{D^0} = S_{\bar{D}^0} = 0$ .

## 2. Angular momentum eigenstates

Let  $\vec{k} = |\vec{k}|(\sin \theta \cos \phi, \sin \theta \sin \phi, \cos \theta)$ , where  $(\theta, \phi)$  are the spherical coordinates of the  $\Lambda$  momentum. The helicity angular-momentum eigenstates are defined by

$$|J_z, \lambda; \Lambda D\rangle = \frac{1}{2\pi} \int d\Omega |\vec{k}, \lambda; \Lambda D\rangle e^{iJ_z \phi} a_{J_z \lambda}^{1/2}(\theta). \quad (\text{A14})$$

Here  $\lambda$  is the helicity of  $\Lambda$ . The helicity basis is related to the spin basis by

$$|\vec{k}, \lambda = \pm 1/2; \Lambda D\rangle = |\vec{k}, \vec{s} = \pm \hat{k}; \Lambda D\rangle, \quad (\text{A15})$$

That is, in a helicity eigenstate, the spin vector  $\vec{s}$  is aligned or anti-aligned with the momentum direction  $\hat{k}$ .

The fixed- $J_z$  helicity states form a complete basis in the  $\Lambda D$  subspace. We therefore introduce

$$\hat{O}_{J_z} = \sum_{\lambda=\pm 1/2} \sum_D \frac{1}{\mathcal{N}_2} |J_z, \lambda; \Lambda D\rangle \langle J_z, \lambda; \Lambda D|, \quad (\text{A16})$$

where  $\mathcal{N}_2 \equiv \langle J_z, \lambda; \Lambda D | J_z, \lambda; \Lambda D \rangle$  is the normalization factor. In the fixed- $J_z$   $\Lambda D$  subspace,  $\hat{O}_{J_z}$  acts as the identity:

$$\langle \vec{k}, \vec{s}; \Lambda D | \mathcal{H}_{\text{eff}} | \Lambda_b, J_z \rangle = \langle \vec{k}, \vec{s}; \Lambda D | \hat{O}_{J_z} \mathcal{H}_{\text{eff}} | \Lambda_b, J_z \rangle. \quad (\text{A17})$$

The unnormalized final state is then

$$|\psi, J_z\rangle_{\text{un}} = \hat{O}_{J_z} \mathcal{H}_{\text{eff}} | \Lambda_b, J_z \rangle = \sum_{\lambda=\uparrow, \downarrow} \sum_D c_{\lambda D} |J_z, \lambda; \Lambda D\rangle. \quad (\text{A18})$$

Here  $\uparrow$  and  $\downarrow$  denote  $\lambda = +1/2$  and  $-1/2$ , respectively. For fixed  $J_z$ , all information about the decay  $\Lambda_b \rightarrow \Lambda D$  is encoded in the four spin–flavor coefficients

$$c_{\lambda D} \equiv \langle J_z = \lambda, \lambda; \Lambda D | \mathcal{H}_{\text{eff}} | \Lambda_b, J_z = \lambda \rangle. \quad (\text{A19})$$

The coefficients  $c_{\lambda D}$  can be obtained from Eq. (A17) by choosing  $\vec{k} = |\vec{k}|\hat{z}$  and  $\vec{s} = \lambda\hat{k}$ . Explicitly,

$$\begin{aligned}\langle \vec{k}, \vec{s}; \Lambda D | \mathcal{H}_{\text{eff}} | \Lambda_b, J_z \rangle &= \frac{1}{\mathcal{N}_2} \langle \vec{k}, \vec{s}; \Lambda D | J_z, \lambda; \Lambda D \rangle \langle J_z, \lambda; \Lambda D | \mathcal{H}_{\text{eff}} | \Lambda_b, J_z \rangle \\ &= \delta_{J_z \lambda} c_{\lambda D}.\end{aligned}\quad (\text{A20})$$

In deriving the last line, we used  $\langle \vec{k}, \vec{s}; \Lambda D | J_z, \lambda; \Lambda D \rangle = \mathcal{N}_2 d_{J_z \lambda}^{1/2}(0)$  and  $d_{J_z \lambda}^{1/2}(0) = \delta_{J_z \lambda}$ . Equations (A20) and (A3) determine the coefficients  $c_{\lambda D}$  in terms of the partial-wave amplitudes  $S_D$  and  $P_D$ , reproducing Eq. (3).

With  $\alpha_D$  and  $\Gamma_D$ , upper and lower bounds on  $\mathcal{C}$  can be obtained from

$$\mathcal{C}_{\text{min,max}} = \frac{2}{\Gamma_{\bar{D}^0} + \Gamma_{D^0}} \left[ \Gamma_{\bar{D}^0} \Gamma_{D^0} - \frac{(\Gamma_{D_1} - \Gamma_{D_2})^2}{4} - \frac{(I_+ \pm I_-)^2}{4} \right]^{1/2}, \quad (\text{A21})$$

where the upper and lower signs correspond to  $\mathcal{C}_{\text{min}}$  and  $\mathcal{C}_{\text{max}}$ , respectively, and

$$I_{\pm} \equiv \left[ \Gamma_{\bar{D}^0} \Gamma_{D^0} (1 \pm \alpha_{\bar{D}^0}) (1 \pm \alpha_{D^0}) - \frac{[\Gamma_{D_1} (1 \pm \alpha_{D_1}) - \Gamma_{D_2} (1 \pm \alpha_{D_2})]^2}{4} \right]^{1/2}. \quad (\text{A22})$$

### Appendix B: Binary Lee–Yang operators in the sampling

The binary nature of the Lee–Yang operators follows from the spin algebra. We use the commutator relations [33]

$$[s_i, s_j] = i\epsilon_{ijk} s_k, \quad [k_i, J_j] = i\epsilon_{ijk} k_k, \quad [s_i, J_j] = i\epsilon_{ijk} s_k. \quad (\text{B1})$$

The local spin components acting on the momentum-helicity state  $|\vec{k}, \lambda; \Lambda D\rangle$  satisfy

$$2s_\theta |\vec{k}, \pm \frac{1}{2}\rangle = |\vec{k}, \mp \frac{1}{2}\rangle, \quad 2s_\phi |\vec{k}, \pm \frac{1}{2}\rangle = \pm i |\vec{k}, \mp \frac{1}{2}\rangle, \quad 2s_r |\vec{k}, \pm \frac{1}{2}\rangle = \pm |\vec{k}, \pm \frac{1}{2}\rangle, \quad (\text{B2})$$

where the label  $\Lambda D$  has been suppressed. The usual spin-1/2 angular-momentum operators act on the  $|J_z, \lambda; \Lambda D\rangle$  basis as

$$J_x |J_z, \lambda\rangle = \frac{1}{2} | -J_z, \lambda\rangle, \quad J_y |J_z, \lambda\rangle = i J_z | -J_z, \lambda\rangle, \quad J_z |J_z, \lambda\rangle = J_z |J_z, \lambda\rangle, \quad (\text{B3})$$

again suppressing the  $\Lambda D$  label. Combining these relations with the Wigner rotation between momentum-helicity states in Eq. (A14) gives

$$\hat{\alpha} |J_z, \lambda\rangle = 2\lambda |J_z, \lambda\rangle, \quad \hat{\gamma} |J_z, \lambda\rangle = |J_z, -\lambda\rangle, \quad \hat{\beta} |J_z, \lambda\rangle = -2i\lambda |J_z, -\lambda\rangle. \quad (\text{B4})$$

The Lee–Yang operators do not change  $J_z$  or  $J$ , since they are rotational scalars satisfying  $[\hat{\xi}, \vec{J}] = 0$ . Therefore, in the  $\Lambda$ -helicity basis,  $\hat{\alpha}$ ,  $\hat{\gamma}$ , and  $\hat{\beta}$  are represented by  $\sigma_z$ ,  $\sigma_x$ , and  $-\sigma_y$ , respectively. In particular,

$$\hat{\xi}^2 = 1, \quad [\hat{\alpha}, \hat{\beta}] = 2i\hat{\gamma}. \quad (\text{B5})$$

Each channel Lee–Yang operator has eigenvalues  $\pm 1$ .

Given an observable  $\hat{O}$ , the statistical uncertainty is governed by  $\sigma_O = \sqrt{(\langle \hat{O}^2 \rangle - \langle \hat{O} \rangle^2) / N}$ , where  $N$  is the number of samples. Suppose that there are  $N_D$  events for  $\Lambda_b \rightarrow \Lambda D$  for a specific flavor  $D$ . If the Lee–Yang operators are measured directly with equal statistics, the uncertainties are

$$\sigma_{\xi_D}^{\text{dir}} = \sqrt{\frac{3(1 - \xi_D^2)}{N_D}}. \quad (\text{B6})$$

In reality, the spin measurements are inferred from the decay  $\Lambda \rightarrow p\pi^-$ , with  $\alpha_\Lambda(\vec{s}) = \langle \hat{p} \rangle$ , where  $\alpha_\Lambda$  is the up-down asymmetry of  $\Lambda \rightarrow p\pi^-$ , and  $\hat{p}$  is the proton momentum direction in the  $\Lambda$  rest frame. Projecting onto the  $D$  channel in Eq. (17), with the normalization  $\langle \hat{O}_D \rangle = 1$ , we obtain

$$\alpha_D = \left\langle \hat{O}_D \frac{3p_r}{\alpha_\Lambda} \right\rangle, \quad \gamma_D = \left\langle \hat{O}_D \frac{-12p_\theta}{\pi p_z \alpha_\Lambda} \right\rangle, \quad \beta_D = \left\langle \hat{O}_D \frac{12p_\phi}{\pi p_z \alpha_\Lambda} \right\rangle. \quad (\text{B7})$$

The corresponding uncertainties are

$$\sigma_{\alpha_D} = \frac{1}{|\alpha_\Lambda|} \sqrt{\frac{3 - \alpha_\Lambda^2 \alpha_D^2}{N_D}}, \quad \sigma_{\gamma_D} = \frac{4}{\pi |p_z \alpha_\Lambda|} \sqrt{\frac{3 - \left(\frac{\pi}{4} p_z \alpha_\Lambda \gamma_D\right)^2}{N_D}}, \quad \sigma_{\beta_D} = \frac{4}{\pi |p_z \alpha_\Lambda|} \sqrt{\frac{3 - \left(\frac{\pi}{4} p_z \alpha_\Lambda \beta_D\right)^2}{N_D}}. \quad (\text{B8})$$

The  $1/|p_z \alpha_\Lambda|$  scaling of the transverse uncertainties reflects that  $\beta_D$  and  $\gamma_D$  enter Eq. (17) only through the  $p_z \sin \theta$  terms and are inferred through the spin-analyzing power  $\alpha_\Lambda$  of  $\Lambda \rightarrow p\pi^-$ .

### Appendix C: Sensitivity to $\gamma$ near the small-concurrence limit

This appendix summarizes how the weak-phase sensitivity is controlled by the spin-flavor concurrence. Flavor-tagged rates and Lee-Yang parameters fix the norms and directions of the helicity spinors  $\chi_D, \chi_{\bar{D}}$ , but not their relative phase. The  $D_1, D_2$  modes and their CP conjugates supply the interference needed to determine that phase together with  $\gamma$ .

In general, the physics is invariant under a  $U(2)$  rotation of the helicity spinors,  $\chi_{\bar{D},D} \rightarrow U \chi_{\bar{D},D}$ . Since  $\chi_{\bar{D},D}$  are determined only up to a relative phase, we can choose the helicity basis such that

$$\chi_{\bar{D}} = \begin{pmatrix} u' \\ 0 \end{pmatrix}, \quad \chi_D = e^{i\phi_u} \begin{pmatrix} u \\ v \end{pmatrix}, \quad u', u, v > 0, \quad (\text{C1})$$

where  $\phi_u$  is the strong phase. Here  $u$  and  $v$  are the positive real components of  $\chi_D$  parallel and perpendicular to  $\chi_{\bar{D}}$ , respectively. We work with normalized amplitudes,  $\mathcal{N} = 1$ . In this basis,

$$u'u = |\chi_{\bar{D}}^\dagger \chi_D| = \frac{1}{2} \sqrt{1 - R_F^2 - \mathcal{C}^2}, \quad u'v = |\chi_{\bar{D}}^T i\sigma_y \chi_D| = \frac{\mathcal{C}}{2}. \quad (\text{C2})$$

The second relation shows that the small-concurrence limit corresponds to a small perpendicular component  $v$ .

We decompose the  $\Lambda_b$  density matrix in flavor space as

$$\rho_{J_z} = \begin{pmatrix} \chi_{\bar{D}} \chi_{\bar{D}}^\dagger & e^{-i\gamma} \chi_{\bar{D}} \chi_D^\dagger \\ e^{i\gamma} \chi_D \chi_{\bar{D}}^\dagger & \chi_D \chi_D^\dagger \end{pmatrix} = \begin{pmatrix} \rho_0 + \rho_z & \rho_x - i\rho_y \\ \rho_x + i\rho_y & \rho_0 - \rho_z \end{pmatrix} \quad (\text{C3})$$

where each  $\rho_i$  is a  $2 \times 2$  matrix in helicity space. The CP-conjugate density matrix is decomposed analogously, with blocks  $\tilde{\rho}_i$ . Since  $\rho_y$  corresponds to the unphysical flavor direction  $D^0 \pm i\bar{D}^0$ , it is not directly observable experimentally. We therefore compare  $\rho_x$  with the CP-conjugate block after applying the helicity flip,  $\tilde{\rho}_x \equiv \sigma_x \tilde{\rho}_x \sigma_x$ .

In the basis above, the off-diagonal helicity entries are

$$(\rho_x)_{12} = \frac{e^{-i(\phi_u + \gamma)}}{2} u'v, \quad (\tilde{\rho}_x)_{12} = \frac{e^{-i(\phi_u - \gamma)}}{2} u'v. \quad (\text{C4})$$

The ratio of the two entries removes the common strong phase  $\phi_u$  and gives

$$\gamma = -\frac{1}{2} \arg \left[ \frac{(\rho_x)_{12}}{(\tilde{\rho}_x)_{12}} \right] \pmod{\pi}. \quad (\text{C5})$$

This modulo- $\pi$  ambiguity is embedded in the parametrization through the simultaneous shift  $\gamma \rightarrow \gamma + \pi$  and  $\phi_u \rightarrow \phi_u + \pi$ , analogous to the usual  $B \rightarrow DK$  ambiguity. The magnitude of each off-diagonal coherence is fixed by the concurrence, given by

$$|(\rho_x)_{12}| = |(\tilde{\rho}_x)_{12}| = \frac{1}{2} u'v = \frac{\mathcal{C}}{4}. \quad (\text{C6})$$

Let  $V_{\text{off}}$  denote the covariance matrix of  $\{\text{Re}(\rho_x)_{12}, \text{Im}(\rho_x)_{12}, \text{Re}(\tilde{\rho}_x)_{12}, \text{Im}(\tilde{\rho}_x)_{12}\}$ . Gaussian error propagation for the phase ratio gives

$$\sigma_{\gamma, \text{off}}^2 = \frac{1}{4} \mathbf{g}^T V_{\text{off}} \mathbf{g} \equiv \frac{\sigma_\xi^2}{\mathcal{C}^2}, \quad \mathbf{g} = \begin{pmatrix} -16 \text{Im}(\rho_x)_{12} / \mathcal{C}^2 \\ 16 \text{Re}(\rho_x)_{12} / \mathcal{C}^2 \\ 16 \text{Im}(\tilde{\rho}_x)_{12} / \mathcal{C}^2 \\ -16 \text{Re}(\tilde{\rho}_x)_{12} / \mathcal{C}^2 \end{pmatrix}. \quad (\text{C7})$$

Here  $\sigma_\xi$  is a finite effective Lee–Yang uncertainty after covariance projection. The factors  $16/\mathcal{C}^2$  in  $\mathbf{g}$  come from differentiating the phase of a complex number with  $|(\rho_x)_{12}| = |(\tilde{\rho}_x)_{12}| = \mathcal{C}/4$ , so that  $1/|(\rho_x)_{12}|^2 = 16/\mathcal{C}^2$ ; the prefactor  $1/4$  is from the square of the  $1/2$  in the phase-ratio extraction.

The diagonal entries also contain the weak phase, but only through cosine constraints. In the same basis,

$$(\rho_x)_{11} = u'u \cos(\gamma + \phi_u), \quad (\tilde{\rho}_x)_{11} = u'u \cos(\phi_u - \gamma). \quad (\text{C8})$$

Since  $u'u$  is fixed by  $R_F$  and  $\mathcal{C}$ , the diagonal entries give the branch-dependent solution

$$\gamma_{\text{diag}} = \frac{1}{2} \left[ \eta_1 \arccos \left( \frac{(\rho_x)_{11}}{u'u} \right) + \eta_2 \arccos \left( \frac{(\tilde{\rho}_x)_{11}}{u'u} \right) \right] \bmod \pi, \quad \eta_1, \eta_2 = \pm 1. \quad (\text{C9})$$

Without knowing the branch signs  $\eta_1$  and  $\eta_2$ , the diagonal constraints give several discrete solutions for  $\gamma$  in  $0 \leq \gamma < \pi$ . Averaging over these unresolved branches would give  $\pi/2$ , independently of the true value of  $\gamma$ , and therefore has no physical meaning as an extraction of the weak phase. Thus the diagonal information alone cannot determine  $\gamma$  unambiguously. The effective precision therefore depends on the off-diagonal phase information, and we parametrize the branch-conditioned contribution by

$$\sigma_{\gamma, \text{diag}}^{\text{eff}} = \frac{f_{\text{br}}(R_F, \mathcal{C})}{\mathcal{C}} \sigma'_\xi. \quad (\text{C10})$$

Here  $\sigma'_\xi$  is the corresponding effective Lee–Yang uncertainty, and  $f_{\text{br}}$  encodes the branch geometry, local slopes, and experimental covariance, which is in general nonzero. The inverse-variance combination with Eq. (C7) gives

$$\sigma_\gamma^{\text{full}} \simeq \frac{1}{\mathcal{C}} \left[ \frac{1}{\sigma_\xi^2} + \frac{1}{f_{\text{br}}^2(R_F, \mathcal{C})(\sigma'_\xi)^2} \right]^{-1/2}. \quad (\text{C11})$$

Thus  $\sigma_\gamma^{\text{full}} \propto \mathcal{C}^{-1}$ , at  $\mathcal{C} \rightarrow 0$ . This scaling should not be extrapolated beyond the Gaussian regime, where the likelihood becomes a mixture over the possible diagonal branches.